

http://pubs.acs.org/journal/aesccq Article

# Formation and Evolution of Catechol-Derived SOA Mass, Composition, Volatility, and Light Absorption

Carley D. Fredrickson, Brett B. Palm, Ben H. Lee, Xuan Zhang, John J. Orlando, Geoffrey S. Tyndall, Lauren A. Garofalo, Matson A. Pothier, Delphine K. Farmer, Zachary C. J. Decker, Michael A. Robinson, Steven S. Brown, Shane M. Murphy, Yingjie Shen, Amy P. Sullivan, Siegfried Schobesberger, and Joel A. Thornton\*



Cite This: ACS Earth Space Chem. 2022, 6, 1067–1079



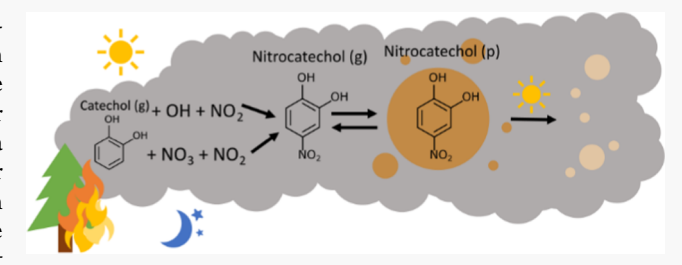
ACCESS

Metrics & More



Supporting Information

ABSTRACT: Phenolic compounds emitted from wildfires contribute to secondary organic aerosol (SOA) and brown carbon (BrC) upon oxidation initiated by hydroxyl (OH) and nitrate radicals (NO<sub>3</sub>). We conducted a set of laboratory chamber experiments to study catechol oxidation by OH and NO<sub>3</sub> with a focus on the associated SOA formation and evolution under conditions relevant to fresh wildfire plumes. Oxidation products in both gas and particle phases as well as SOA volatility were measured using an iodide-adduct high-resolution time-of-flight



chemical ionization mass spectrometer coupled with the filter inlet for gases and aerosols (FIGAERO-CIMS). Nitrocatechol ( $C_6H_5NO_4$ ) was the dominant particle-phase compound in both OH-initiated and NO<sub>3</sub>-initiated oxidation and was strongly associated with particle light absorption at 405 nm, consistent with BrC. Maximum SOA mass yields, ranging from 0.1 to 1.6 for the OH- and NO<sub>3</sub>-driven experiments, respectively, varied with the net formation of nitrocatechol. Gas-particle partitioning measurements implied the effective saturation vapor concentration,  $c^*$ , of nitrocatechol is 12  $\mu$ g m<sup>-3</sup> for the OH-initiated experiment and 2.4  $\mu$ g m<sup>-3</sup> for the NO<sub>3</sub>-initiated experiments, both far lower than group contribution method estimates, which ranged from 1.8  $\times$  10<sup>2</sup> to 8.5  $\times$  10<sup>8</sup>  $\mu$ g m<sup>-3</sup>. In extended photochemical aging experiments, wall-loss-corrected photochemical lifetimes of BrC in the chamber were 17.4  $\pm$  0.8 and 12.4  $\pm$  0.1 h, while particulate nitrocatechol had lifetimes of 21  $\pm$  8 and 6.9  $\pm$  0.6 h for OH-initiated and NO<sub>3</sub>-initiated conditions, respectively. Implications for phenolic-derived SOA and BrC evolution in wildfire plumes are discussed.

KEYWORDS: phenolic compounds, biomass burning, secondary organic aerosol, gas—particle partitioning, wildfire smoke, nitroaromatics, nitrocatechol

#### 1. INTRODUCTION

Wildfires emit carbon dioxide, carbon monoxide, methane, black carbon, primary organic aerosol (POA), reactive nitrogen oxides (NO<sub>x</sub> = NO + NO<sub>2</sub>), and volatile organic compounds (VOCs), among other components, to the atmosphere. The gaseous and particulate emissions and secondary pollutants such as ozone and secondary organic aerosol (SOA) adversely affect human health, impair visibility, and impact climate. SOA formation, evolution, and properties in wildfire plumes remain uncertain due, in part, to uncertain oxidation conditions, complex distributions of volatile, intermediate, and semivolatile (VOC, IVOC, SVOC) precursors, POA and SOA loss processes, and chemical drivers of optical properties such as brown carbon (BrC), a component of OA that strongly absorbs in the ultraviolet and visible wavelengths.  $^{3,9,11}$ 

Phenolic compounds, classified by the presence of a benzene ring with at least one hydroxy substituent, are emitted during biomass burning, are highly reactive to OH and NO<sub>3</sub>, and can contribute to SOA and BrC formation. 12-14 Gas-phase oxidation of phenolic compounds by the hydroxyl radical (OH) produces SOA with yields ranging from 0.003 to 1.45. 15-19 A few of these studies also incorporate NO<sub>x</sub>, which in turn produces substantial nitroaromatic compounds and SOA with BrC. 15,20,21 The oxidation of phenolic compounds with NO<sub>3</sub> under dark conditions has been relatively understudied, but previous work has shown associated SOA mass yields as high as 161%, rich in nitroaromatic compounds and with significant BrC character. 13,15,22

Received: January 5, 2022 Revised: March 18, 2022 Accepted: March 22, 2022 Published: March 31, 2022





Nitroaromatic compounds are toxic, mutagenic, and carcinogenic  $^{23-26}$  and strongly absorb UV—vis radiation, thereby contributing to BrC. Their formation in a wildfire plume due to phenolic oxidation is thus a source of secondary BrC. Mohr et al.  $^{12}$  showed that just a few nitrated phenolic compounds measured in authentic biomass burning aerosol can explain at least 5–10% of biomass burning aerosol light absorption at 370 nm. Nitroaromatics are likely formed in high yield in the first generation of oxidation of most phenolic compounds under high-NO $_x$  conditions; such products are expected to be of intermediate volatility based on structure—activity relationships. Additionally, nitroaromatics have been shown to be photochemically labile, contributing to mass loss of these compounds as a result of photochemical aging.  $^{27-29}$  As such, the importance of their contribution to SOA and BrC as a wildfire plume dilutes and ages remains uncertain.

Understanding the yields, gas-particle partitioning, and fate of nitroaromatics formed from phenolic oxidation under wildfire plume conditions is of interest to simulating associated SOA and its optical properties. However, there are relatively few independent studies of photochemical and nocturnal oxidation of phenolic compounds under the high-NO<sub>x</sub> conditions of a fresh wildfire plume and fewer still that probe evolution with extended photochemical aging. While BrC is being incorporated into global climate models, the yields, lifetimes, and optical properties of SOA and BrC from wildfire smoke chemistry have not been extensively quantified under nighttime conditions. Moreover, it remains unclear whether photochemistry or nocturnal chemistry of phenolic compounds is a more efficient source of BrC and whether the associated BrC is long-lived under typical atmospheric conditions. 30-32

We present results from laboratory chamber studies of catechol (C<sub>6</sub>H<sub>6</sub>O<sub>2</sub>) oxidation and associated SOA and BrC molecular and optical properties. These chamber studies are motivated by the findings of the Western wildfire Experiment for Cloud chemistry, Aerosol absorption and Nitrogen (WE-CAN) aircraft field campaign that studied the chemistry, composition, and properties of wildfire smoke in the western United States. During this field campaign, an iodide-adduct high-resolution time-of-flight chemical ionization mass spectrometer (I- HR-ToF-CIMS) reported a rapid loss of catechol (and isomers) with plume aging for multiple fires, which was again observed during the Fire Influence on Regional to Global Environments and Air Quality (FIREX-AQ) field campaign. 9,33,34 Moreover, the WE-CAN analysis suggested phenolic compounds, including catechol, contributed the most to estimated SOA formation from primary emitted gaseous precursors in the sampled wildfire plumes. With high concentrations of NO<sub>x</sub> and limited photochemistry in optically thick plumes, catechol is expected to react with both NO3 and OH.<sup>34</sup> Using the National Center for Atmospheric Research (NCAR) environmental chamber, we quantified gas-phase and particle-phase composition, absorption, volatility, and evolution of SOA formed from OH and NO3 oxidation of catechol under conditions relevant to wildfire smoke and conducive to aging.

#### 2. METHODS

**2.1. MOONLIGHT Chamber Experiment and Instrumentation Overview.** The Monoterpene and Oxygenated Aromatics Oxidation at Night and Under Lights (MOONLIGHT) project was a multi-institution collaboration to

investigate the daytime (OH-initiated) and nighttime (NO<sub>3</sub>initiated) oxidation of a specific subset of VOCs emitted by biomass burning. It was conducted from May to June 2019, in part to complement the findings from WE-CAN. No unexpected or unusually high safety hazards were encountered. Biomass burning relevant VOCs studied during MOON-LIGHT consisted of phenolics and furans: phenol, catechol, cresol, guaiacol, and furfural. Experiments were conducted within NCAR's 10 m<sup>3</sup> FEP Teflon chamber<sup>35</sup> housed in a cubic enclosure with UV-reflective surfaces surrounded by 128 blacklight tubes (32W, Type F32T8/BL). The NO<sub>2</sub> photolysis frequency,  $j_{NO_2}$ , was measured to be 1.24  $\times$  10<sup>-3</sup> s<sup>-1</sup> at 100% light intensity. The chamber temperature was kept at a constant 295 K when the blacklights were off and increased to  $\sim$ 305 K when the blacklights were operated at full capacity. All reactants and products were passively mixed within the chamber. For catechol experiments, the relative humidity of the chamber was kept below 10% and ammonium sulfate dry seeds with a monomodal size distribution and maximum mass at a vacuum aerodynamic diameter of 350 nm were injected to compete with sorption of organic vapors onto the chamber walls. At the end of each experiment, the chamber was cleaned overnight or longer by flowing zero air through it with the lights off.

Measurements of bulk submicron OA, sulfate aerosol (pSO<sub>4</sub>), and ammonium aerosol (pNH<sub>4</sub>) were performed by the Aerosol Mass Spectrometer (HR-AMS; Aerodyne Research, Inc.),<sup>36</sup> hereafter abbreviated as AMS, or the Aerosol Chemical Speciation Monitor (ACSM).<sup>37</sup> While the AMS is generally considered a PM1 instrument because the lens transmits most ambient particles less than 1  $\mu$ m, the actual 50% transmission is typically around a vacuum aerodynamic diameter of 750 nm.  $^{38,39}$  AMS mass concentrations ( $\mu g \text{ m}^{-3}$ ) were converted to  $\mu g \text{ sm}^{-3}$  by adjusting to standard pressure (101.3 kPa) while the temperature was not adjusted for. We assumed a temperature of 295 K in the chamber, and given the variations during the experiments, AMS mass concentrations do not change by more than 5%. Measurements of ozone were made by a UV-absorption ozone monitor (Model 49i-PIS, Thermo Scientific), while NO and NO2 were measured with a chemical luminescence NO detector (Model CLD 88Y, EcoPhysics) coupled with a customized external LED photolytic NO<sub>2</sub>/NO convertor. Additional measurements of NO, NO<sub>2</sub>, NO<sub>3</sub>, N<sub>2</sub>O<sub>5</sub>, NO<sub>1</sub>, and ozone (O<sub>3</sub>) were also performed by the National Oceanic and Atmospheric Administration's nitrogen oxide cavity ring-down spectrometer. 40 A multichannel photoacoustic spectrometer (PAS) provided by the University of Wyoming, as described in Foster et al., 41 was used to measure dry aerosol absorption at 405 and 660 nm. Colorado State University's Particle-into-Liquid-Sampler-Liquid Waveguide Capillary Cell-Total Organic Carbon (PILS-LWCC-TOC) instrument measured the water-soluble BrC absorption at 405 nm and the water-soluble organic carbon (WSOC) concentration. 42 Both the PAS and PILS-LWCC-TOC used URG sharp-cut Teflon coated aluminum cyclones, URG-2000-30ED at a flow rate of 5.7 L min<sup>-1</sup> and URG-2000-30EHB at a flow rate of 16.7 L min<sup>-1</sup>, respectively, to realize particle size cut-points of 1  $\mu$ m aerodynamic diameter. Since we performed chemical experiments instead of field measurements or burn experiments, there is no absorption contribution from black carbon in our

Table 1. Chamber Conditions for All Catechol Oxidation Experiments

expt. no.	1	2	3	4	5
experiment description	daytime	dark formation with photochemical aging	dark formation with extended photochemical aging	dark formation with extended photochemical aging without oxidants	dark formation and aging (no lights)
temperature range (°C)	23-35	22.5-35	22.5-35	22.7-36	22.6-23
relative humidity (%)	<10	<10	<10	<10	<10
initial oxidant type	OH	$NO_3$	$NO_3$	$NO_3$	$NO_3$
duration (h)	6.65	3.83	18.67	18.38	20.08
time until lights on for aging (min)		136	99	153	
reacted catechol ( $\mu g \text{ sm}^{-3}$ )	112	33.3	90.0	110	49.9
seed concentration preoxidant ( $\mu g \text{ sm}^{-3}$ )	62	101	115	94	160
AMS <sup>a</sup> maximum w.l.c. OA produced ( $\mu$ g sm <sup>-3</sup> )	>30	>36	>52	>46	>57
FIGAERO maximum OA produced (µg sm <sup>-3</sup> )	16	46	114	153	78
AMSa SOA yield	>0.27	>1.08	>0.58	>0.42	>1.14
FIGAERO-CIMS SOA yield	0.14	1.38	1.27	1.39	1.56

<sup>a</sup>For Expt. 5, an ACSM was used instead of an AMS.

chamber. Thus, we can ascribe total absorption at  $405~\mathrm{nm}$  to BrC absorption.

Measurements of gas-phase and particle-phase composition of oxygenated compounds were performed by the FIGAERO (Filter Inlet for Gases and Aerosols) I HR-ToF-CIMS, which will hereafter be referred to as the FIGAERO-CIMS. 43,44 The FIGAERO-CIMS was largely operated as in Lopez-Hilfiker et al.,44 and here, we summarize key points and differences from the previous operations. The FIGAERO-CIMS has two operating modes switching one after the other: gas-phase mode and particle-phase mode. In gas-phase sampling mode, gases are measured with the I- HR-ToF-CIMS while concurrently in a separate inlet, particles are being collected on a Teflon filter. No cyclones are used with the FIGAERO-CIMS, thus the FIGAERO-CIMS has no imposed size cut. This mode ran in 10-min increments with background gasphase measurements being conducted every 2 min to quantify the background signal originating from the ion-molecule reaction (IMR) region.<sup>45</sup> In particle-phase sampling mode, heated ultrahigh-purity N2 is pulled through the particle-laden filter to be sampled by the I HR-ToF-CIMS, and its temperature slowly increases from 20 to 200 °C at a rate of 10 °C min<sup>-1</sup>. This heating evaporates compounds with different volatilities off the filter at different temperatures and is known as thermal desorption. The thermal desorption is followed by a soak period where the temperature is saturated at 200 °C for 32 min. After the soak period, there is a 10-min cooldown period prior to starting the next sampling cycle. The particle-phase mode ran in 60-min increments where every fourth particle desorption was a particle blank, where a second filter was placed upstream of the FIGAERO collection filter such that no particles were collected during the sampling phase. Particle blanks were linearly interpolated and subsequently subtracted from the normal particle desorption signals. For nitrocatechol, we assessed what fraction the particle blank contributed to the total particle-phase signal and subtracted that fraction, which is not the typical linear interpolation approach and assumes that the magnitude of the blank scales with the previous amount of nitrocatechol sampled. The uncertainties from particle-blank subtraction will be larger for rapidly changing conditions, like during the first

couple of hours after experiment start in the chamber experiments.

The sensitivity of nitrocatechol for the I- HR-ToF-CIMS and FIGAERO-CIMS was determined by injecting diluted solutions of nitrocatechol, acetone, and methanol onto a poly(tetrafluoroethylene) filter already positioned within our sampling tube while actively sampling into the I HR-ToF-CIMS. During the sampling, we flowed ultrahigh-purity nitrogen gas into the IMR region for 6 s every 2 min to measure the amount of background signal originating from IMR off-gassing, a method known as the fast-zero method.<sup>45</sup> The gas-phase sensitivity was computed as in Palm et al., eq 1.45 For the particle-phase sensitivity, the fast-zero background correction is not applied since FIGAERO-CIMS thermal desorptions cannot implement the fast-zero method. With a known mass of nitrocatechol injected, integrating the I- HR-ToF-CIMS signal allows for a determination of the sensitivity. The sensitivity of catechol and 4-nitrophenol was determined similarly except for the following differences. The catechol solution was composed of catechol and acetone and the 4nitrophenol solution was composed of 4-nitrophenol and acetone. Additional catechol and 4-nitrophenol calibration experiments were performed while injecting water vapor into the sample flow resulting in a ratio of roughly 0.4  $IH_2O^-/I^-$ , and a water vapor correction equation for the sensitivities was determined. Another catechol calibration experiment was conducted by evaporating solid catechol contained in a Teflon cup. We applied instrument-specific sensitivity values of 11.8 normalized counts per second (ncps)/ppt to particle-phase nitrocatechol and  $C_{12}H_{10}N_2O_8$  ( $T_{max}$  evaluated to be two nitrocatechols), 33.7 ncps/ppt to particle-phase nitrophenol, 4.6 ncps/ppt to gas-phase nitrocatechol, and 12.2 ncps/ppt to water-vapor-corrected gas-phase catechol. All sensitivities have a calibration uncertainty of 30%. When a compound's sensitivity was not known, an empirical value of 5 ncps/ppt was used, though this estimate has little impact on our conclusions. Particle-phase measurements were converted from counts to  $\mu g$  m<sup>-3</sup> using the particle-phase sensitivities, compound molecular weights, and standard pressure and temperature (298 K).

Five experiments with catechol were conducted. The first experiment was initiated with OH as the target oxidant with 6.7 h of photochemical aging (Expt. 1), whereas the remaining experiments were initiated with NO<sub>3</sub> as the target oxidant (Expts. 2–5) with differing aging schemes. The first NO<sub>3</sub>-initiated experiment was followed by 1.6 h of photochemical aging (Expt. 2). The next experiment repeated Expt. 2 but had 17 h of photochemical aging (Expt. 3). Another NO<sub>3</sub>-initiated experiment had 17.7 h of photochemical aging without the oxidants O<sub>3</sub> and OH through injections of excess NO and 2-butanol (Expt. 4). Finally, there was a NO<sub>3</sub>-initiated experiment with 20.6 h of aging in the dark without oxidants O<sub>3</sub> and OH (Expt. 5). More information on each experiment's conditions is provided in Table 1.

In Figures 1 and 2, we illustrate the progress of experiments and observations using Expts. 1 (OH +  $NO_x$ ) and 3 ( $NO_3$  +

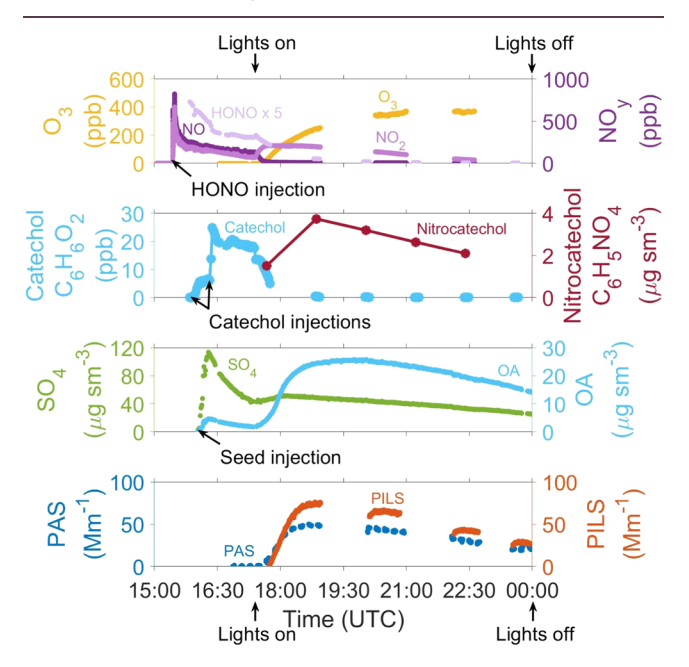


**Figure 1.** Absorption at 405 nm as measured by the PAS and PILS-LWCC-TOC (labeled PILS);  $O_3$ , NO, and NO<sub>2</sub> as measured by the NOAA nitrogen oxide cavity ring-down spectrometer; AMS  $pSO_4$  and AMS OA; and particle-phase nitrocatechol and gas-phase catechol from the FIGAERO-CIMS are plotted across four windows for Expt. 1 (OH + NO<sub>x</sub>). Chamber events are labeled with arrows and descriptive text.

long photochemical ( $h\nu$ ) aging) as examples. Measurements of the equilibrium NO<sub>3</sub> are presented in Figure S1 and ranged from 0 to 115 ppt across all of the experiments. In Expt. 1 (OH +  $NO_x$ ), hydrogen peroxide ( $H_2O_2$ ), nitrous acid (HONO), catechol, and ammonium sulfate seed were injected before the lights were turned on to generate OH and NO. HONO was generated by reacting 3 mL 10% by weight sulfuric acid and 3 mL 1% by weight sodium nitrite, adapted from the method of Cox and Derwent. 46 This reaction also produces NO<sub>x</sub>, as observed prior to the lights being turned on. When the lights turned on, absorption at 405 nm as measured by the PAS and PILS-LWCC-TOC increased as well as O3, AMS OA, and particle-phase nitrocatechol, while catechol decreased. In Expt. 3 (NO<sub>3</sub> + long h $\nu$  aging), O<sub>3</sub>, catechol, and ammonium sulfate seed aerosol were injected. Catechol + O<sub>3</sub> is known to make SOA<sup>47</sup> and we observed this OA before NO<sub>2</sub> was added. Once NO<sub>2</sub> was injected, NO<sub>3</sub> was produced from the reaction of

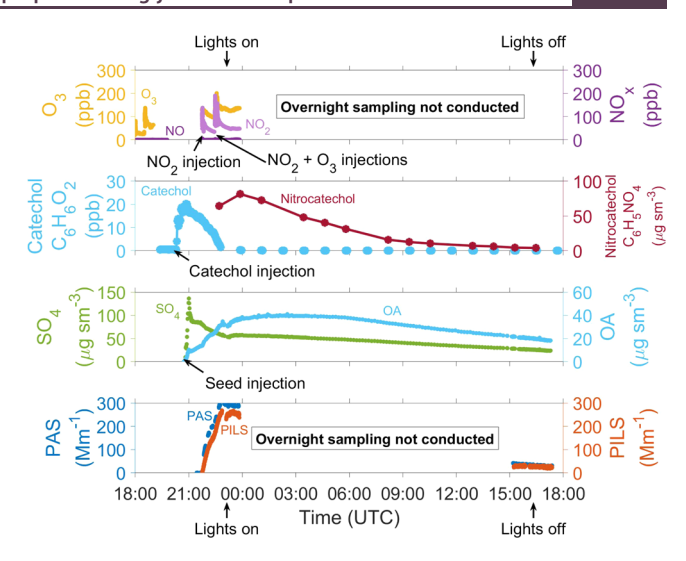


**Figure 2.** Similar to Figure 1, but for Expt. 3 (NO<sub>3</sub> + long h $\nu$  aging).

 $NO_2$  and  $O_3$ . Following  $NO_2$  injection, absorption at 405 nm, AMS OA, and nitrocatechol all increased as catechol decreased. To observe the effects of photochemistry, the lights were turned on for 17 h. Due to volumetric sampling constraints, the PAS, PILS-LWCC-TOC, and the NOx and  $O_3$  instruments did not sample the chamber for most of this photochemistry. The PAS and PILS-LWCC-TOC started sampling again after 15.68 h with the lights on.

2.2. SOA Yield and Volatility. The SOA mass yield is defined as the mass concentration of the newly formed organic aerosol ( $\Delta C_{OA}$ ) divided by the mass of the reacted VOC ( $\Delta$ VOC). In these experiments,  $\Delta C_{OA}$  was determined with wall-loss-corrected (w.l.c.) OA measurements from the AMS and  $\Delta$ VOC was estimated with the gas-phase measurement of catechol from the FIGAERO-CIMS. The wall-loss correction was implemented by finding the decay rate of the bulk AMS pSO<sub>4</sub> aerosol in each experiment and adding the lost OA mass back to the baseline measurements. Since the ammonium sulfate dry aerosol seed was the only source of sulfate aerosol in the chamber, the decay of sulfate aerosol as measured by the AMS was solely due to wall loss and gravitational settling. We also used non-wall-loss-corrected FIGAERO-CIMS OA to determine  $\Delta C_{OA}$  and calculate a different SOA mass yield for reasons discussed in Section 3.1. We also quantified the molar yield of individual compounds by dividing the observed change in the molar concentration of the product by the change in the molar concentration of the reactant.

The volatility of the SOA formed in the experiments was diagnosed using the FIGAERO-CIMS temperature-programmed thermal desorptions, which produce thermograms, the detected ion signals of compounds as a function of the desorption temperature. The thermogram is a measure of a compound's propensity to evaporate from the collected particles as a function of temperature, and thus is related to effective volatility. The temperature at which the desorption signal reaches a maximum is denoted as  $T_{\rm max}$ . This property has previously been found to correlate with a compound's enthalpy of sublimation and saturation vapor pressure for approximately ideal mixtures. Herther discussion of FIGAERO thermogram volatility measurements can be found in Section S1 and Figures S2–S4. While  $T_{\rm max}$  correlates with enthalpy of sublimation and saturation vapor pressure, it does not predict these properties without proper calibration and

given nonidealities likely in realistic organic aerosol systems as well as thermal decomposition during the desorption process. With the aid of a theoretical evaporation model framework designed to interpret FIGAERO-CIMS data as discussed further in Section S2, experimental results can be compared to the theoretical output. A demonstrated example is provided in Figure S5.

We also utilized gas-particle partitioning theory 49-52 applied to nitrocatechol observations in the gas and particle phases made with the FIGAERO-CIMS, as described in Section 3, for comparison of effective saturation vapor concentration,  $c^*$ , to a suite of predictions by group contribution methods. While the FIGAERO-CIMS thermal desorptions are reproducible across experiments and instruments, there are limitations to these experimental methods for volatility estimates as discussed by Lopez-Hilfiker et al. 44,53,54 and Stark et al.<sup>55</sup> For example, thermal decomposition of lower volatility components in the SOA can lead to estimates of volatility that are biased high. 53,54 Additionally, Stark et al. 55 found that using measurements to calculate gas-particle partitioning can result in a skewed volatility distribution, due to signal-to-background limits of instruments, which will vary for each compound and instrument. This issue also leads to estimates of saturation vapor concentrations that may be biased high.

Evaluated group contribution methods included EVAPO-RATION, by Compernolle et al., 56 the Myrdal and Yalkowsky method,<sup>57</sup> the method of Nannoolal et al.,<sup>58</sup> and SIMPOL.1 by Pankow and Asher.<sup>59</sup> The Myrdal and Yalkowsky,<sup>57</sup> Nannoolal,<sup>58</sup> and EVAPORATION vapor pressure estimations for individual compounds were computed with the University of Manchester's UManSysProp: Multiphase system online property prediction tool (http://umansysprop.seaes. manchester.ac.uk/tool/vapour pressure), using the Nannoolal<sup>60</sup> boiling point method. The Joback and Reid<sup>61</sup> boiling point method has previously been shown to overestimate the boiling point, and the Nannoolal<sup>60</sup> boiling point method has been shown to exhibit the lowest mean bias error for the methods considered here. 62,63 For each of the group contribution methods that use a SMILES string as input, nitrocatechol's SMILES string was sourced from the Master Chemical Mechanism (MCM), O=N(=O)c1ccc(O)c(O)c1. SIMPOL.1's calculation of the volatility of nitrocatechol was done in three ways as Pankow and Asher<sup>59</sup> do not explicitly define how a compound like nitrocatechol is to be treated and is further described in Section S3. Only the low- and highvolatility values from these calculations are included in the analysis hereafter. We emphasize that all group contribution methods used for this research heavily lack representation from functionalized nitroaromatic compounds.

## 3. RESULTS AND DISCUSSION

**3.1. SOA Yields.** SOA mass yields and molar yields for nitrocatechol ( $C_6H_5NO_4$ ) for Expts. 1–5 are summarized in Tables 1 and S1, respectively. Though ammonium sulfate seed was added to mitigate loss of vapors to the chamber walls, this wall loss could still be occurring and thus our SOA mass and molar yields are lower estimates. The same can be said about FIGAERO OA mass and molar yields, as the FIGAERO-CIMS OA is not wall-loss-corrected and is discussed below. Our SOA yields for each catechol—oxidant pair experiment ranged from minimums of 0.27 to 1.14 for AMS-derived OA and from 0.14 to 1.56 for FIGAERO-CIMS-derived OA. These results

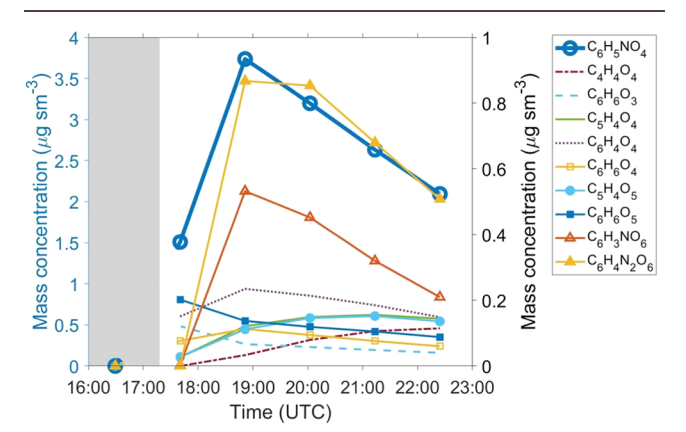
confirm that SOA mass formation from oxygenated aromatics, likely important components of S/IVOC not only in wildfire plumes but also urban areas, can be highly efficient, especially in the presence of high  $NO_x$ . Our nitrocatechol molar yields for each catechol—oxidant pair experiment ranged from 0.02 in the OH-initiated experiment to 0.81 in the  $NO_3$ -initiated experiments. Further discussion of nitrocatechol molar yields can be found in Section S4.

Maximum OA produced in the experiments as measured by the AMS and FIGAERO-CIMS differed. As shown in sizeresolved chemical composition measurements by Garofalo et al., 64 the nitrocatechol produced in the NO<sub>3</sub>-initiated oxidation experiments (Expts. 2–5) selectively condensed to larger particle sizes due to exclusion by existing SOA produced by ozonolysis of catechol. Consequently, the nitrocatecholcontaining aerosol mode most likely spans the upper size range cutoffs of the AMS, as well as perhaps the PAS and PILS-LWCC-TOC. Therefore, using AMS OA for SOA yields may not be appropriate as the actual size distribution of the particles was unknown and corrections for transmission efficiencies would introduce additional unconstrained uncertainties. Nitrocatechol condensation likely increased particle size beyond the 750 nm vacuum aerodynamic diameter size cut of the AMS aerodynamic lens, whereas the FIGAERO-CIMS had no imposed size cut, causing the discrepancy in maximum OA mass concentrations. Particle bounce in the AMS is another possible contributor to the different temporal evolution in OA mass and properties, but we were unable to evaluate its importance. Therefore, the reported SOA mass yields using AMS OA are lower limits. Given that the majority of SOA in these NO<sub>3</sub>-initiated experiments was composed of nitrocatechol, with some OA produced by ozonolysis of catechol, as will be discussed in Section 3.2, the direct calibration of the FIGAERO-CIMS to nitrocatechol thereby provides a reasonably accurate measure of total catechol + NO<sub>3</sub>-derived SOA mass. The FIGAERO-CIMS maximum OA mass concentration is consistently larger than that determined by the AMS for NO<sub>3</sub>-initiated oxidation experiments (Expts. 2-5). However, the FIGAERO-CIMS OA cannot be corrected for wall loss as AMS pSO<sub>4</sub> does not capture the larger nitrocatechol-containing particles. For the reasons discussed above, the FIGAERO-CIMS-derived SOA mass yields are more accurate for these NO<sub>3</sub>-initiated experiments due to the starting seed size and the heterogeneous nucleation of nitrocatechol to an independent size mode.

Finewax et al.<sup>15</sup> previously reported catechol SOA yields ranging from 1.11 to 1.45 for OH-initiated oxidation and 1.38 to 1.61 for NO<sub>3</sub>-initiated oxidation. The FIGAERO-CIMSderived SOA yields are in good agreement with the NO3initiated oxidation but not the OH-initiated oxidation (Expt. 1). Citing one reason for this difference, Finewax et al. 15 used dioctyl sebacate (DOS) seed aerosol instead of ammonium sulfate seed aerosol. It is possible that having the added organic absorbing medium in the seed enhanced yields compared to having an inorganic seed.<sup>65</sup> SOA yield is also affected by oxidant exposure. The Finewax et al. 15 study also differed in the amounts of reacted catechol and NO<sub>x</sub>, reacting up to 56 times more catechol than our experiments and up to 100 times more NO<sub>x</sub>. The catechol and NO<sub>x</sub> concentrations used within the NCAR chamber were based on those measured in fresh wildfire smoke during the WE-CAN campaign. 9,66 Lower concentrations of catechol and NOx could lead to faster removal of nitrocatechol and SOA in our experiments

compared to that of Finewax et al. 15 and thus lower net SOA yields in the OH-initiated experiments.

**3.2.** Particle Composition of Catechol-Derived SOA. The 10 particle-phase compounds detected by the FIGAERO-CIMS having the highest increasing mass-weighted signal for Expt. 1 (OH + NO<sub>x</sub>) and Expt. 3 (NO<sub>3</sub> + long h $\nu$  aging) are shown in Figure 3. The mass spectra of organic compounds at



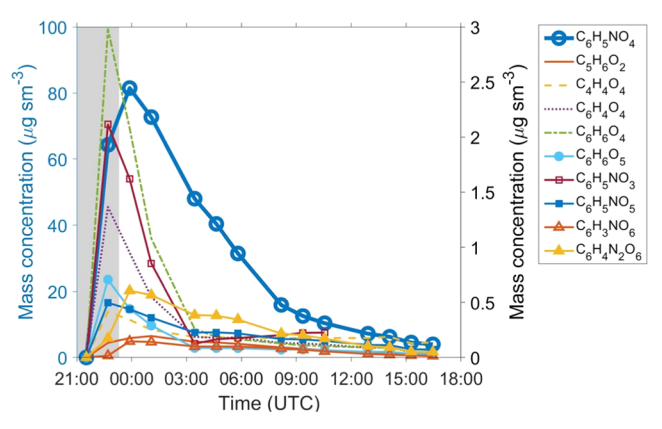


**Figure 3.** Time series of the notable increasing particle-phase compounds in two experiments. Top: Catechol + OH + NO $_x$  (Expt. 1). Bottom: Catechol + NO $_3$  + long h $\nu$  aging (Expt. 3). Nitrocatechol ( $C_6H_5NO_4$ ) is plotted on the blue left y-axis for both plots, and all other compounds are plotted on the black right y-axis. Gray shading indicates when the lights were off. No line connects the data from pre-lights to post-lights in Expt. 1 (OH + NO $_x$ ) because particulate compounds are generated after lights were on.

the time of peak OA mass concentration for Expts. 1 and 3 are provided in Figure S6. For Expt. 1 (OH + NO<sub>x</sub>), the most intense individual ion from the FIGAERO-CIMS was C<sub>6</sub>H<sub>5</sub>NO<sub>4</sub>I<sup>-</sup>, the ion-adduct of nitrocatechol, which increased after the lights turned on producing OH and NO via H2O2 and HONO photolysis. Net production of nitrocatechol ceased when catechol was consumed and subsequently decreased over time for the rest of the experiment during which the chamber UV lights remained on to continue producing OH radicals, mostly from residual HONO and H2O2 photolysis and partly from ozone photolysis. In addition to nitrocatechol, other particle-phase compounds with carbon number 4  $(C_4)$  to  $C_6$ were observed to grow in at differing times, indicating the evolution of particle composition with oxidative aging, albeit at relatively much lower abundance than nitrocatechol. C<sub>6</sub>H<sub>4</sub>N<sub>2</sub>O<sub>6</sub>, presumably a di-nitro-catechol isomer, was the second largest compound to grow in after lights on, and subsequently, more oxidized nitrogen-containing compounds

grew in, such as  $C_6H_3NO_6$ . Notably, a set of non-N-containing  $C_4-C_6$  were produced, some showing significant oxidation and potential retainment of aromaticity, such as  $C_6H_6O_5$ . These are unlikely to be fragments upon further inspection of each compound's thermograms. In Expt. 1 (OH +  $NO_x$ ), more than half of the FIGAERO-CIMS detected SOA mass was distributed over many low abundance components across a large range of compositions, suggesting a greater degree of complexity to OH-initiated oxidation compared to  $NO_3$ -initiated chemistry discussed below. This is also evident given the lower overall molar yield of nitrocatechol in Finewax et al.  $^{15}$  and in this work.

In Expt. 3 (NO<sub>3</sub> + long h $\nu$  aging), nitrocatechol was the dominant particle-phase compound detected by the FIG-AERO-CIMS for the entire experiment comprising more than 70% of the OA at maximum OA mass concentrations, even more so than in Expt. 1 (OH +  $NO_x$ ). Many of the top 10 compounds were C<sub>6</sub> compounds, both with and without nitrogen. While particulate nitrocatechol slowly decayed over the course of the experiment, many C<sub>6</sub> particulate compounds like C<sub>6</sub>H<sub>6</sub>O<sub>4</sub>, C<sub>6</sub>H<sub>4</sub>O<sub>4</sub>, and C<sub>6</sub>H<sub>6</sub>O<sub>5</sub> were produced quickly at the start of the experiment but decayed to near-background after only 4 h. Other particulate compounds decayed relatively slower than nitrocatechol, such as C<sub>6</sub>H<sub>4</sub>N<sub>2</sub>O<sub>6</sub>, C<sub>6</sub>H<sub>5</sub>NO<sub>5</sub>, C<sub>4</sub>H<sub>4</sub>O<sub>4</sub>, and C<sub>6</sub>H<sub>3</sub>NO<sub>6</sub>. While distributed differently, there were many overlapping compounds between Expts. 1 (OH +  $NO_x$ ) and 3 ( $NO_3$  + long  $h\nu$  aging). Besides nitrocatechol,  $C_6H_4O_4$ ,  $C_6H_6O_5$ ,  $C_6H_3NO_6$ , and  $C_6H_4N_2O_6$  are in the top 10 highest signal compounds in the particle phase for both experiments. Expt. 1 (OH + NO $_x$ ) has more C<sub>4</sub> and C<sub>5</sub> compounds consistent with a greater degree of ring-opening and C-C bond scission pathways during OH-initiated oxidation compared to NO<sub>3</sub>.

**3.3. Constraints on Nitrocatechol c\*.** We observed nitrocatechol to have the largest FIGAERO-CIMS signal for any individual compound in all of the catechol oxidation experiments we conducted. However, the volatility, and thus phase, of nitrocatechol is poorly constrained. A compound's phase is an important factor for determining its atmospheric lifetime, dictating reaction rates with other oxidants as well as wet and dry deposition rates. Moreover, to generalize SOA formation from aromatics, having accurate volatility distributions of the major oxidation products is required. These chamber experiments provided an opportunity to assess the volatility of nitrocatechol under atmospherically relevant conditions.

Assuming particles achieved gas—particle equilibrium in the chamber, we used gas—particle partitioning theory based on Raoult's law, eq 1, together with measurements of gas- and particle-phase concentrations of nitrocatechol and of total OA mass concentrations to estimate the  $c^*$  of nitrocatechol

$$\frac{c_i^{\mathrm{P}}}{c_i^{\mathrm{g}}} \sim \frac{c_{\mathrm{OA}}}{\gamma_i c_i^{\mathrm{o}}} = \frac{c_{\mathrm{OA}}}{c_i^*} \tag{1}$$

where  $c_i^p$  is the mass concentration of compound i in the particle phase,  $c_i^g$  is the mass concentration of compound i in the gas phase,  $c_i^o$  is the saturation vapor concentration relative to the pure substance,  $\gamma_i$  is the activity coefficient for nonideality, and  $c_{OA}$  is the total absorbing organic aerosol mass concentration. Note for our purposes of estimation, we assumed that the molecular masses of OA and compound i are the same and that  $\gamma_i \sim 1$ . For these conditions and for all

subsequent analyses, we used the observed total FIGAERO-CIMS OA and the gas- and particle-phase mass concentrations of nitrocatechol from each FIGAERO-CIMS desorption period to solve for the inferred nitrocatechol  $c^*$ .

The gas-particle partitioning-derived  $c^*$  estimates for nitrocatechol are shown in Figure 4. In Expt. 1 (OH +

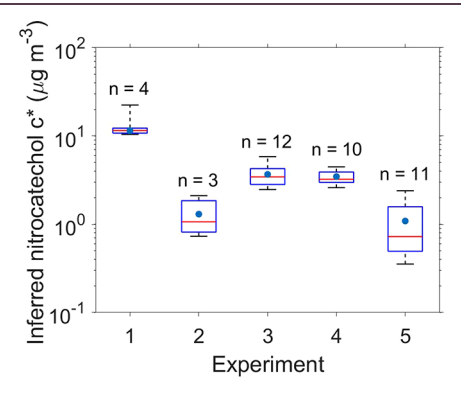


**Figure 4.** Box plot of the solved nitrocatechol effective saturation vapor concentrations,  $c^*$ , for every desorption within each catechol experiment using gas—particle partitioning theory. The red line in the box plot is the median, and the blue dot is the mean. The Expt. 1 (OH + NO<sub>x</sub>) upper whisker is the mean  $c^*$  computed using AMS OA since the chamber particles were smaller than 1  $\mu$ m and fully detectable by the AMS.

 $NO_x$ ), the average  $c^*$  was 12  $\mu$ g m<sup>-3</sup>, which was outside the upper limits of the other experiments but comparable to the Finewax et al. estimate of 13  $\mu$ g m<sup>-3</sup> considering the likely order of magnitude uncertainties associated with the methodology. The average  $c^*$  for Expts. 2 through 5 (NO<sub>3</sub> oxidation) ranged from 1 to 4  $\mu$ g m<sup>-3</sup>. We show how representative these average values are for each experiment at every desorption in Figure S7. Expts. 3 (NO<sub>3</sub> + long h $\nu$  aging) and 4 (NO<sub>3</sub> + long  $h\nu$  aging – oxidants) had the lowest spread of nitrocatechol  $c^*$ estimates of the NO<sub>3</sub>-initiated experiments, whereas Expt. 1  $(OH + NO_x)$  had the lowest spread of nitrocatechol  $c^*$  of all of the experiments. Expt. 2 (NO<sub>3</sub> + short h $\nu$  aging) lacked aging conditions to potentially lower the spread and Expt. 5 (NO<sub>3</sub> + long dark aging) showed a near-monotonic decline in estimated  $c^*$  over time, as shown in Figure S8. We note that, in theory, there should only be a single c\* value for nitrocatechol for a given set of conditions, e.g., T, P, total OA, OA composition, and phase state. The fact that the estimate for c\* varies between experiments and within an experiment is partly due to variations in the properties of the OA as it ages, such as viscosity and composition, which would affect partitioning, in addition to chamber condition variations. As shown in Figure S5 and discussed in Section S2, the FIGAERO-CIMS thermograms suggest a nitrocatechol c\* that is at most 5  $\mu$ g m<sup>-3</sup>, with the thermogram model assuming that nitrocatechol-containing particles had grown beyond 1  $\mu$ m. Thus, the experimental evidence suggests an effective nitrocatechol c\*, e.g., which includes effects of accretion reactions and viscosity, that is less than 12  $\mu g \ m^{-3}$  and within aged particles evolves to be potentially less than 1  $\mu$ g m<sup>-3</sup>. To explain significant nitrocatechol in particles detected at total organic aerosol mass concentrations less than 30  $\mu g$  m<sup>-3</sup> in Expt. 1, we require a lower effective  $c^*$ . For comparison, Booth et al.<sup>68</sup> measured the saturation vapor pressure of nitrocatechol over the pure solid to be 2.6  $\mu$ g m<sup>-3</sup> and estimated a value of

62  $\mu$ g m<sup>-3</sup> relative to a subcooled liquid, where their difference may be attributed to their viscosities. Notably, their solid-state  $c^{\circ}$  is on the same order of magnitude as our  $c^{*}$  estimates for the NO<sub>3</sub>-initiated experiments, in which nitrocatechol was the dominant particle component, i.e., approaching the pure substance. In the OH-initiated experiment, nitrocatechol was part of a more complex particle composition with an unknown phase state.

We compare the experimental estimates of nitrocatechol  $c^*$  to those estimated by multiple group contribution methods in Figure 5. The group contribution methods as a whole greatly

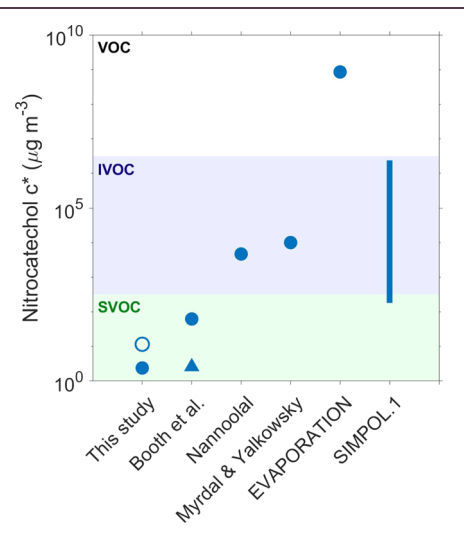


**Figure 5.** Estimated nitrocatechol effective saturation vapor concentrations,  $c^*$ , using different vapor pressure group contribution methods. This study's gas—particle partitioning method is the average of the OH-initiated (open circle) and NO<sub>3</sub>-initiated (closed circle) solved  $c^*$  from Figure 4. Previous literature from Booth et al. <sup>68</sup> reports  $c^*$  for solid state (triangle) and subcooled liquid state (circle). Nannoolal <sup>58</sup> and Myrdal and Yalkowsky <sup>57</sup>  $c^*$  estimates were calculated with the Nannoolal <sup>60</sup> boiling point estimation method. SIMPOL.1 presented a range of values depending on the contribution of the aromatic hydroxyls. Volatility classes are colored and labeled in the background as in Chuang and Donahue. <sup>69</sup>

overestimated nitrocatechol c\* compared to the experimental estimates, with ranges from  $10^2$  to  $10^9$   $\mu$ g m<sup>-3</sup>. The group contribution methods Nannoolal<sup>58</sup> and Myrdal and Yalkowsky<sup>57</sup> yielded similar  $c^*$  of  $4.7 \times 10^3$  and  $1.0 \times 10^4 \ \mu g \ m^{-3}$ , respectively. The EVAPORATION method had reported the highest volatility of nitrocatechol at  $8.5 \times 10^8 \ \mu g \ m^{-3}$ . SIMPOL.1 had ranged from  $1.8 \times 10^2$  to  $2.4 \times 10^6 \ \mu g \ m^{-3}$ , depending upon the choice of functional group combinations. We note that if we used the Joback and Reid<sup>61</sup> boiling point method with the Nannoolal group contribution method, we were able to produce a nitrocatechol  $c^*$  of 3  $\mu$ g m<sup>-3</sup>, on the same order as the experimental estimates. These results indicate that for modeling organic volatility distributions in both wildfire plumes and urban areas, there is a significant need to improve saturation vapor pressure estimates for functionalized aromatics. An expanded version of Figure 5 including different boiling point methods and SMILES strings is provided in Figure S9.

**3.4. Evolution of Particle Light Absorption.** Nitrocatechol absorbs strongly in the near-UV region<sup>70–72</sup> and thus will contribute to BrC.<sup>3</sup> Here, we examine the extent to which the evolutions of particulate nitrocatechol concentrations and

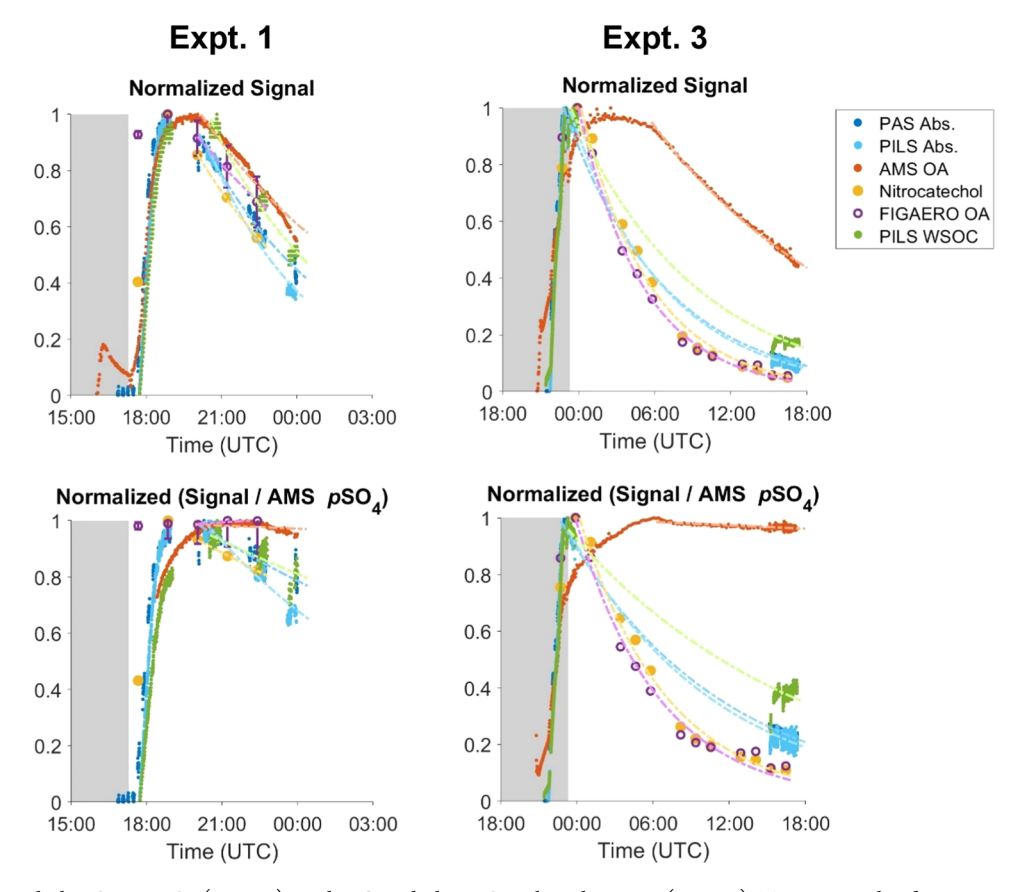


Figure 6. Left: Catechol + OH + NO<sub>x</sub> (Expt. 1). Right: Catechol + NO<sub>3</sub> + long h $\nu$  aging (Expt. 3). Top: Normalized time series of the absorption as measured by the PAS at 405 nm and PILS-LWCC-TOC (here, PILS); mass concentrations of AMS OA, particle-phase nitrocatechol, and FIGAERO-CIMS OA (with uncertainties of FIGAERO-CIMS OA calculation from nitrocatechol particle-blank subtraction in Expt. 1 only); and the concentration of WSOC from the PILS. Bottom: The same measurements divided by AMS  $pSO_4$  and then normalized. Exponential decay fits of each variable are plotted as dashed lines. Lifetimes,  $\tau$ , of all fits are reported in Table 2.

UV-vis absorption are related to evaluate mechanisms governing BrC lifetimes. Figure 6 (top left) shows the normalized evolutions of PAS and PILS-LWCC-TOC absorption at 405 nm, AMS OA, particle-phase nitrocatechol, FIGAERO-CIMS total OA, and PILS-LWCC-TOC WSOC during Expt. 1 (OH +  $NO_r$ ). The unnormalized evolutions are shown in Figure S10. For this experiment only, the FIGAERO-CIMS total OA was calculated with nitrocatechol using the linear particle-blank subtraction method instead of the fraction particle-blank subtraction method described in Section 2.1. This was a more appropriate method since only one particleblank desorption occurred in this experiment. The AMS OA and particle-phase nitrocatechol followed a similar trend as the PAS and PILS-LWCC-TOC absorption, but the particle-phase nitrocatechol peaked at the same time as the PAS and PILS-LWCC-TOC absorption and followed their decay shapes more closely. To account for the decay contributed by particle loss to the chamber walls, we divide these measurements by the AMS pSO<sub>4</sub>. Since there is no evidence that particles grew outside of the AMS upper size cut in Expt. 1, all particle wall loss is accounted for across all measurements. We found that after 21:00 UTC, the AMS OA/AMS pSO<sub>4</sub> remained roughly constant in time, indicating that no net OA was being formed or lost. The FIGAERO-CIMS total OA/AMS pSO<sub>4</sub> yields the same pattern. However, PAS absorption/AMS pSO<sub>4</sub> and nitrocatechol/AMS pSO<sub>4</sub> decayed with continued photochemical aging. The PILS-LWCC-TOC absorption/AMS pSO<sub>4</sub> had the fastest decay. Given this correlated evolution,

and that particle-phase nitrocatechol accounts for the most FIGAERO-CIMS OA mass concentration as an individual compound, we believe nitrocatechol, or oligomers which decompose into nitrocatechol during thermal desorption, may be responsible for the bulk of particle light absorption formed in this experiment.

Comparing the evolution of normalized nitrocatechol, PAS and PILS-LWCC-TOC absorption at 405 nm, AMS OA, FIGAERO-CIMS OA, and PILS-LWCC-TOC WSOC for Expt. 3 (NO<sub>3</sub> + long h $\nu$  aging) is not as straightforward compared to Expt. 1. Nitrocatechol selectively condensed to larger particles most likely spanning the upper range cutoffs of the AMS, and perhaps the PAS and the PILS-LWCC-TOC. Therefore, the decays reported by these instruments are likely influenced by relative transmission efficiencies of the different instruments, and thus not representative of the total particulate matter. With this caveat in mind, we see that the absorption generally followed the particle-phase nitrocatechol, FIGAERO-CIMS total OA (primarily nitrocatechol), and PILS-LWCC-TOC WSOC, and not AMS OA, as shown in Figure 6 (top right). The unnormalized evolutions are shown in Figure S11. Since both the PAS and PILS-LWCC-TOC measurements generally followed the FIGAERO-CIMS measurements and not AMS OA, the difference between the AMS and all other instruments is due to the lower size cut at 750 nm vacuum aerodynamic diameter, but perhaps also due to additional OA formed after catechol depletion. Normalizing these measurements by AMS  $pSO_4$  comes with similar caveats to above. As

some pSO<sub>4</sub> grew outside the AMS size cut, pSO<sub>4</sub> is underestimated and would make pSO<sub>4</sub> decays appear faster than the truth and lead to over-correcting for particle wall loss. This bias would lead to decays that are slower than in reality. Normalized particle-phase nitrocatechol/AMS pSO<sub>4</sub> in the bottom right, decayed quicker than, but similar to light absorption/AMS pSO<sub>4</sub>, and AMS total OA/AMS pSO<sub>4</sub> changed relatively little 6.68 h after lights on. PAS and PILS-LWCC-TOC absorption are highly correlated in time with particulate nitrocatechol mass concentration even when the AMS OA mass concentration was not, regardless of normalization to AMS pSO<sub>4</sub> to account for particle wall loss. We cannot definitively conclude that particulate nitrocatechol determines the evolution of BrC, as measured by PAS and PILS-LWCC-TOC 405 nm absorption, formed from catechol oxidation by OH or NO<sub>3</sub> under high-NO<sub>x</sub> conditions (NO<sub>x</sub> > 10 ppb). However, since nitrocatechol comprises more than 70% of the FIGAERO-CIMS OA at peak OA mass, it is likely to be the key compound. Secondary oxidation of O<sub>3</sub>-oxidation products could be responsible for additional OA production.

The lifetime of PAS 405 nm light absorption, our proxy for BrC, normalized to AMS  $pSO_4$  is ~17 and 12 h in Expts. 1  $(OH + NO_x)$  and 3  $(NO_3 + long h\nu aging)$ , respectively. However, the lifetime of nitrocatechol in the FIGAERO-CIMS normalized to AMS pSO<sub>4</sub> is roughly 2 times shorter in Expt. 3  $(NO_3 + long h\nu aging)$ , where SOA was formed by  $NO_3$ chemistry without lights followed by photochemical aging with lights on as seen in Table 2. Normalizing lifetimes to AMS pSO<sub>4</sub> is a way to account for loss of particles to the chamber walls but will serve as upper limits for the NO3-initiated experiments where particles grew outside of the AMS size range. Looking at unnormalized lifetimes still incorporates the particle wall loss process, but also may not be representative of all particles in the NO3-initiated experiments as mentioned previously. Due to chamber volume sampling restrictions, we do not have PAS light absorption data during overnight portions of the experiments that would further constrain the exponential fits. There are a few possible explanations for the shorter lifetime of particulate nitrocatechol in Expt. 3 (NO<sub>3</sub> + long  $h\nu$  aging) compared to Expt. 1 (OH + NO<sub>x</sub>). One possibility could be particle morphology, as, unlike in Expt. 3  $(NO_3 + long h\nu aging)$ , the Expt. 1  $(OH + NO_r)$  SOA was a more complex composition where nitrocatechol made up less than half of total FIGAERO-CIMS OA. Such a situation could lead to reduced rates of evaporation to the gas phase if particlephase nitrocatechol were buried and unable to access the surface due to diffusion limitations. In addition, differences between AMS OA, PAS light absorption, and FIGAERO mass concentration measurements may also be explained in part to different dependencies on particle size. In Expt. 3 ( $NO_3$  + long  $h\nu$  aging), particles containing nitrocatechol grew beyond the ammonium sulfate mode to above 750 nm where differences in instrument particle transmission may affect apparent time series of the measured variables as particles evaporate and or settle during aging. These larger nitrocatechol-containing particles in Expt. 3 (NO<sub>3</sub> + long h $\nu$  aging) would also have a faster gravitational settling time than those in Expt. 1 (OH + NO<sub>x</sub>) and will be reflected in our derived lifetimes. With all biases stated previously, the range of lifetimes reported between those that are pSO<sub>4</sub>-normalized and unnormalized are likely the best estimates of the actual photochemical lifetimes.

Table 2. Lifetimes and Confidence Intervals of the Decay Fits of PAS and PILS-LWCC-TOC (Here PILS) Absorption, AMS OA, Nitrocatechol, FIGAERO OA, and PILS

	PAS absorption	PILS absorption	AMS <sup>d</sup> OA	nitrocatechol	FIGAERO OA	PILS WSOC
expt. 1 lifetime (h)	$5.3 \pm 0.1$	$4.08 \pm 0.05$	$7.7 \pm 0.2$	6 ± 3	a	$5.2 \pm 0.1$
expt. 1 pSO <sub>4</sub> -normalized lifetime (h)	$17.4 \pm 0.8$	$9.7 \pm 0.3$	$260 \pm 90$	$21 \pm 8$	a	$22 \pm 1$
expt. 2 lifetime (h)	$4.4 \pm 0.2$	$4.3 \pm 0.1$	$18 \pm 2$	ь	Ь	$4.04 \pm 0.05$
expt. 2 pSO <sub>4</sub> -normalized lifetime (h)	$8.6 \pm 0.6$	$9.1 \pm 0.5$	a	b	b	$7.5 \pm 0.1$
expt. 3 lifetime (h)	$7.9 \pm 0.1$	$7.43 \pm 0.03$	$15.7 \pm 0.1$	$5.6 \pm 0.6$	$5.1 \pm 0.3$	$9.83 \pm 0.02$
expt. 3 pSO <sub>4</sub> -normalized lifetime (h)	$12.4 \pm 0.1$	$11.5 \pm 0.1$	$490 \pm 80$	$6.9 \pm 0.6$	$6.5 \pm 0.7$	$18.4 \pm 0.1$
expt. 4 lifetime (h)	$6.8 \pm 0.2$	a	$9.5 \pm 0.2 (11.2 \pm 0.5, 10.4 \pm 0.1)^{c}$	$8 \pm 1 \ (12 \pm 5, 6.2 \pm 0.2)^c$	$7.6 \pm 0.8 \ (9 \pm 3, 6.1 \pm 0.4)^{c}$	$7.2 \pm 0.1$
expt. 4 pSO <sub>4</sub> -normalized lifetime (h)	$11.4 \pm 0.2$	a	$43 \pm 1 (120 \pm 60, 38 \pm 1)^c$	$19 \pm 8  (^a, 10.5 \pm 0.7)^c$	$17 \pm 5  (^a, 10 \pm 1)^c$	$17.8 \pm 0.2$
expt. 5 lifetime (h)	$4.6 \pm 0.1$	$4.01 \pm 0.05$	$3.9 \pm 0.1$	$4.2 \pm 0.2$	$3.6 \pm 0.1$	$3.73 \pm 0.04$
expt. 5 pSO <sub>4</sub> -normalized lifetime (h)	a	$16 \pm 1$	$28 \pm 1$	a	a	$12.0 \pm 0.5$
"Not distinguishable from 0, so lifetim	a undefined bant e	nough data noints t	and distinguishable from 0 on lifetime undefined bnot enging the committe lifetime. That a necknown injection and nost-huranol injection lifetimes. After Frant 5 an ACSM was used	l injection, and post-butanol inj	ection lifetimes dEor Exnt S an	ACSM was used

inguishable an AMS. instead of

There are several processes that could be driving the observed decays in nitrocatechol and light absorption. Photolysis, gas-phase nitrocatechol oxidation, and vapor wall loss followed by repartitioning are possible contributors. Further experiments on particulate nitroaromatic chemical and physical evolution that control for vapor wall interactions are needed.

#### 4. CONCLUSIONS

A suite of group contribution methods failed to predict a nitrocatechol c\* within the range of the observational estimates, generally higher by 2 or more orders of magnitude, though these methods have real-world atmospheric chemistry modeling applications. EVAPORATION is used in the F0AM-WAM model<sup>73</sup> and has also been used with the CMAQv5.2 $\gamma$ model<sup>74</sup> and SPectral Aerosol Cloud Chemistry Interaction Model (SPACCIM)<sup>75</sup> and SIMPOL.1 is easily coupled to the MCM.  $^{76,77}$  Thus, there is a need to revisit  $c^*$  estimation methods for oxidized and nitrated aromatic compounds. Our experimental results suggest that nitrocatechol will partition predominantly into the particle phase, especially in wildfire smoke plumes but will be subject to significant dynamic repartitioning upon plume dilution. Differences in nitrocatechol c\* estimations may be attributed to particle viscosity. If so, relative humidity may play an important factor and needs to be studied in the future.

Photochemical aging of the catechol-derived SOA led to continuous loss of nitrocatechol particle mass, as well as BrC absorption at 405 nm, at rates that exceeded seed particle wall loss rates. The BrC light absorption measured by PAS decayed via photochemical aging with a lifetime of ~17 and ~12 h in OH- and NO<sub>3</sub>-initiated SOA chamber experiments, respectively. These chamber lifetimes are similar to previously reported lifetimes of BrC in transported wildfire smoke, but our chamber lifetimes will need to be translated to atmospheric lifetimes for further comparison.<sup>30</sup> We expect lifetimes to be longer in the atmosphere as our oxidant concentrations were higher in the chamber and wall loss occurred in the chamber. A more thorough experiment isolating each reaction pathway is required to estimate atmospheric lifetimes. However, the observed particulate nitrocatechol decay upon photochemical aging differed between experiments, exhibiting a lifetime of roughly 21 h when formed from OH chemistry and ~7 h from dark chemistry. While generally consistent with the measured BrC lifetimes, the more rapid loss of nitrocatechol suggests the potential for additional contributors to 405 nm light absorption than nitrocatechol alone.

Nitroaromatics such as nitrocatechol are not only present in biomass burning smoke but can arise from the oxidation of anthropogenic emissions of aromatics associated with fossil fuel use and volatile consumer products (VCP). Nitroaromatics are thus also likely important in urban SOA. Based on our findings, it is possible that air quality models may be underestimating an anthropogenic SOA source if not tracking the multigenerational aging of aromatics. In addition, nitroaromatics are used in pesticides, dyes, explosives, pharmaceuticals, and chemical industries, and such knowledge of their  $c^*$  will help determine emissions from these potential source categories. Previous research studying the volatility of the aerosol in these urban environments using group contribution methods will likely need to be reevaluated.

#### ASSOCIATED CONTENT

## **Solution** Supporting Information

The Supporting Information is available free of charge at https://pubs.acs.org/doi/10.1021/acsearthspace-chem.2c00007.

Molar yields of nitrocatechol, descriptions of FIGAERO thermograms and volatility, description of the thermogram model, and description of the calculation of nitrocatechol volatility with SIMPOL.1 (Table S1 and Figures S1–S11) (PDF)

#### AUTHOR INFORMATION

## **Corresponding Author**

Joel A. Thornton — Department of Atmospheric Sciences, University of Washington, Seattle, Washington 98195, United States; orcid.org/0000-0002-5098-4867; Email: thornton@atmos.uw.edu

#### **Authors**

Carley D. Fredrickson – Department of Atmospheric Sciences, University of Washington, Seattle, Washington 98195, United States; © orcid.org/0000-0002-9127-5258

Brett B. Palm — Department of Atmospheric Sciences, University of Washington, Seattle, Washington 98195, United States; Present Address: Atmospheric Chemistry Observations and Modeling Laboratory, National Center for Atmospheric Research, Boulder, Colorado 80301, United States

Ben H. Lee – Department of Atmospheric Sciences, University of Washington, Seattle, Washington 98195, United States

Xuan Zhang — Atmospheric Chemistry Observations and Modeling Laboratory, National Center for Atmospheric Research, Boulder, Colorado 80301, United States; Present Address: Department of Life and Environmental Sciences, University of California, Merced, Merced, California 95343, United States.

John J. Orlando – Atmospheric Chemistry Observations and Modeling Laboratory, National Center for Atmospheric Research, Boulder, Colorado 80301, United States

Geoffrey S. Tyndall – Atmospheric Chemistry Observations and Modeling Laboratory, National Center for Atmospheric Research, Boulder, Colorado 80301, United States

Lauren A. Garofalo – Department of Chemistry, Colorado State University, Fort Collins, Colorado 80523, United States; © orcid.org/0000-0001-7593-2580

Matson A. Pothier – Department of Chemistry, Colorado
State University, Fort Collins, Colorado 80523, United States

Delphine K. Farmer – Department of Chemistry, Colorado State University, Fort Collins, Colorado 80523, United States; © orcid.org/0000-0002-6470-9970

Zachary C. J. Decker — NOAA Chemical Sciences Laboratory, Boulder, Colorado 80305, United States; Cooperative Institute for Research in Environmental Sciences, University of Colorado, Boulder, Colorado 80309, United States; Department of Chemistry, University of Colorado, Boulder, Colorado 80309-0215, United States; Present Address: Paul Scherrer Institute (PSI), Laboratory for Atmospheric Chemistry, Villigen 5232, Switzerland.;

Michael A. Robinson – NOAA Chemical Sciences Laboratory, Boulder, Colorado 80305, United States; Cooperative Institute for Research in Environmental Sciences, University of

- Colorado, Boulder, Colorado 80309, United States; Department of Chemistry, University of Colorado, Boulder, Colorado 80309-0215, United States
- Steven S. Brown NOAA Chemical Sciences Laboratory, Boulder, Colorado 80305, United States; Department of Chemistry, University of Colorado, Boulder, Colorado 80309-0215, United States; orcid.org/0000-0001-7477-9078
- Shane M. Murphy Department of Atmospheric Science, University of Wyoming, Laramie, Wyoming 82071, United States
- Yingjie Shen Department of Atmospheric Science, University of Wyoming, Laramie, Wyoming 82071, United States
- Amy P. Sullivan Department of Atmospheric Science, Colorado State University, Fort Collins, Colorado 80523, United States
- Siegfried Schobesberger Department of Applied Physics, University of Eastern Finland, Kuopio 70211, Finland

Complete contact information is available at: https://pubs.acs.org/10.1021/acsearthspacechem.2c00007

#### Notes

The authors declare no competing financial interest.

#### ACKNOWLEDGMENTS

This project was entirely funded by the National Science Foundation through Grant Number NSF AGS 1652688. C.D.F., B.B.P., and J.A.T. acknowledge support from the National Oceanic and Atmospheric Administration for the FIREX-AQ campaign with the NOAA OAR Climate Program Office Award Number NA17OAR4310012. C.D.F. additionally acknowledges the National Aeronautics and Space Administration with the Future Investigators in NASA Earth and Space Science and Technology (FINESST) Grant Number 80NSSC20K1612. The National Center for Atmospheric Research is operated by the University Corporation for Atmospheric Research under the sponsorship of the National Science Foundation. L.A.G., M.A.P., and D.K.F. acknowledge the NOAA OAR Climate Program Office Award Number NA17OAR4310010. S.S. acknowledges support by the Academy of Finland (Grant Number 310682).

### REFERENCES

- (1) Akagi, S. K.; Yokelson, R. J.; Wiedinmyer, C.; Alvarado, M. J.; Reid, J. S.; Karl, T.; Crounse, J. D.; Wennberg, P. O. Emission Factors for Open and Domestic Biomass Burning for Use in Atmospheric Models. *Atmos. Chem. Phys.* **2011**, *11*, 4039–4072.
- (2) Bond, T. C.; Doherty, S. J.; Fahey, D. W.; Forster, P. M.; Berntsen, T.; DeAngelo, B. J.; Flanner, M. G.; Ghan, S.; Kärcher, B.; Koch, D.; Kinne, S.; Kondo, Y.; Quinn, P. K.; Sarofim, M. C.; Schultz, M. G.; Schulz, M.; Venkataraman, C.; Zhang, H.; Zhang, S.; Bellouin, N.; Guttikunda, S. K.; Hopke, P. K.; Jacobson, M. Z.; Kaiser, J. W.; Klimont, Z.; Lohmann, U.; Schwarz, J. P.; Shindell, D.; Storelvmo, T.; Warren, S. G.; Zender, C. S. Bounding the Role of Black Carbon in the Climate System: A Scientific Assessment: BLACK CARBON IN THE CLIMATE SYSTEM. J. Geophys. Res. 2013, 118, 5380–5552.
- (3) Laskin, A.; Laskin, J.; Nizkorodov, S. A. Chemistry of Atmospheric Brown Carbon. *Chem. Rev.* **2015**, *115*, 4335–4382.
- (4) Andreae, M. O. Emission of Trace Gases and Aerosols from Biomass Burning an Updated Assessment. *Atmos. Chem. Phys.* **2019**, *19*, 8523–8546.
- (5) Andreae, M. O.; Merlet, P. Emission of Trace Gases and Aerosols from Biomass Burning. *Global Biogeochem. Cycles* **2001**, *15*, 955–966.

- (6) Buysse, C. E.; Kaulfus, A.; Nair, U.; Jaffe, D. A. Relationships between Particulate Matter, Ozone, and Nitrogen Oxides during Urban Smoke Events in the Western US. *Environ. Sci. Technol.* **2019**, 53, 12519–12528.
- (7) Jaffe, D. A.; Wigder, N. L. Ozone Production from Wildfires: A Critical Review. *Atmos. Environ.* **2012**, *51*, 1–10.
- (8) Koss, A. R.; Sekimoto, K.; Gilman, J. B.; Selimovic, V.; Coggon, M. M.; Zarzana, K. J.; Yuan, B.; Lerner, B. M.; Brown, S. S.; Jimenez, J. L.; Krechmer, J.; Roberts, J. M.; Warneke, C.; Yokelson, R. J.; de Gouw, J. Non-Methane Organic Gas Emissions from Biomass Burning: Identification, Quantification, and Emission Factors from PTR-ToF during the FIREX 2016 Laboratory Experiment. *Atmos. Chem. Phys.* 2018, 18, 3299–3319.
- (9) Palm, B. B.; Peng, Q.; Fredrickson, C. D.; Lee, B. H.; Garofalo, L. A.; Pothier, M. A.; Kreidenweis, S. M.; Farmer, D. K.; Pokhrel, R. P.; Shen, Y.; Murphy, S. M.; Permar, W.; Hu, L.; Campos, T. L.; Hall, S. R.; Ullmann, K.; Zhang, X.; Flocke, F.; Fischer, E. V.; Thornton, J. A. Quantification of Organic Aerosol and Brown Carbon Evolution in Fresh Wildfire Plumes. *Proc. Natl. Acad. Sci. U.S.A.* 2020, 117, 29469—29477.
- (10) Karanasiou, A.; Alastuey, A.; Amato, F.; Renzi, M.; Stafoggia, M.; Tobias, A.; Reche, C.; Forastiere, F.; Gumy, S.; Mudu, P.; Querol, X. Short-Term Health Effects from Outdoor Exposure to Biomass Burning Emissions: A Review. *Sci. Total Environ.* **2021**, *781*, No. 146739.
- (11) Garofalo, L. A.; Pothier, M. A.; Levin, E. J. T.; Campos, T.; Kreidenweis, S. M.; Farmer, D. K. Emission and Evolution of Submicron Organic Aerosol in Smoke from Wildfires in the Western United States. *ACS Earth Space Chem.* **2019**, *3*, 1237–1247.
- (12) Mohr, C.; Lopez-Hilfiker, F. D.; Zotter, P.; Prévôt, A. S. H.; Xu, L.; Ng, N. L.; Herndon, S. C.; Williams, L. R.; Franklin, J. P.; Zahniser, M. S.; Worsnop, D. R.; Knighton, W. B.; Aiken, A. C.; Gorkowski, K. J.; Dubey, M. K.; Allan, J. D.; Thornton, J. A. Contribution of Nitrated Phenols to Wood Burning Brown Carbon Light Absorption in Detling, United Kingdom during Winter Time. *Environ. Sci. Technol.* **2013**, 47, 6316–6324.
- (13) Bolzacchini, E.; Bruschi, M.; Hjorth, J.; Meinardi, S.; Orlandi, M.; Rindone, B.; Rosenbohm, E. Gas-Phase Reaction of Phenol with NO 3. *Environ. Sci. Technol.* **2001**, *35*, 1791–1797.
- (14) The Mechanisms of Atmospheric Oxidation of Aromatic Hydrocarbons; In Calvert, J. G., Ed.; Oxford University Press: Oxford, 2002.
- (15) Finewax, Z.; de Gouw, J. A.; Ziemann, P. J. Identification and Quantification of 4-Nitrocatechol Formed from OH and NO <sub>3</sub> Radical-Initiated Reactions of Catechol in Air in the Presence of NO <sub>x:</sub> Implications for Secondary Organic Aerosol Formation from Biomass Burning. *Environ. Sci. Technol.* **2018**, *52*, 1981–1989.
- (16) Lauraguais, A.; Coeur-Tourneur, C.; Cassez, A.; Deboudt, K.; Fourmentin, M.; Choël, M. Atmospheric Reactivity of Hydroxyl Radicals with Guaiacol (2-Methoxyphenol), a Biomass Burning Emitted Compound: Secondary Organic Aerosol Formation and Gas-Phase Oxidation Products. *Atmos. Environ.* **2014**, *86*, 155–163.
- (17) Nakao, S.; Clark, C.; Tang, P.; Sato, K.; Cocker, D., III Secondary Organic Aerosol Formation from Phenolic Compounds in the Absence of NOx. *Atmos. Chem. Phys.* **2011**, *11*, 10649–10660.
- (18) Pereira, K. L.; Hamilton, J. F.; Rickard, A. R.; Bloss, W. J.; Alam, M. S.; Camredon, M.; Ward, M. W.; Wyche, K. P.; Muñoz, A.; Vera, T.; Vázquez, M.; Borrás, E.; Ródenas, M. Insights into the Formation and Evolution of Individual Compounds in the Particulate Phase during Aromatic Photo-Oxidation. *Environ. Sci. Technol.* **2015**, 49, 13168–13178.
- (19) Yee, L. D.; Kautzman, K. E.; Loza, C. L.; Schilling, K. A.; Coggon, M. M.; Chhabra, P. S.; Chan, M. N.; Chan, A. W. H.; Hersey, S. P.; Crounse, J. D.; Wennberg, P. O.; Flagan, R. C.; Seinfeld, J. H. Secondary Organic Aerosol Formation from Biomass Burning Intermediates: Phenol and Methoxyphenols. *Atmos. Chem. Phys.* **2013**, 13, 8019–8043.
- (20) Lin, P.; Liu, J.; Shilling, J. E.; Kathmann, S. M.; Laskin, J.; Laskin, A. Molecular Characterization of Brown Carbon (BrC)

- Chromophores in Secondary Organic Aerosol Generated from Photo-Oxidation of Toluene. *Phys. Chem. Chem. Phys.* **2015**, *17*, 23312–23325.
- (21) Romonosky, D. E.; Laskin, A.; Laskin, J.; Nizkorodov, S. A. High-Resolution Mass Spectrometry and Molecular Characterization of Aqueous Photochemistry Products of Common Types of Secondary Organic Aerosols. *J. Phys. Chem. A* **2015**, *119*, 2594–2606.
- (22) Mayorga, R. J.; Zhao, Z.; Zhang, H. Formation of Secondary Organic Aerosol from Nitrate Radical Oxidation of Phenolic VOCs: Implications for Nitration Mechanisms and Brown Carbon Formation. *Atmos. Environ.* **2021**, 244, No. 117910.
- (23) Kovacic, P.; Somanathan, R. Nitroaromatic Compounds: Environmental Toxicity, Carcinogenicity, Mutagenicity, Therapy and Mechanism: Nitro Aromatic Pollutants. *J. Appl. Toxicol.* **2014**, 34, 810–824.
- (24) Kroflič, A.; Grilc, M.; Grgić, I. Does Toxicity of Aromatic Pollutants Increase under Remote Atmospheric Conditions? *Sci. Rep.* **2015**, *5*, No. 8859.
- (25) Leuenberger, C.; Czuczwa, J.; Tremp, J.; Giger, W. Nitrated Phenols in Rain: Atmospheric Occurrence of Phytotoxic Pollutants. *Chemosphere* **1988**, *17*, 511–515.
- (26) Traversi, D.; Degan, R.; De Marco, R.; Gilli, G.; Pignata, C.; Villani, S.; Bono, R. Mutagenic Properties of PM2.5 Urban Pollution in the Northern Italy: The Nitro-Compounds Contribution. *Environ. Int.* **2009**, *35*, 905–910.
- (27) Malecha, K. T.; Cai, Z.; Nizkorodov, S. A. Photodegradation of Secondary Organic Aerosol Material Quantified with a Quartz Crystal Microbalance. *Environ. Sci. Technol. Lett.* **2018**, *5*, 366–371.
- (28) Baboomian, V. J.; Gu, Y.; Nizkorodov, S. A. Photodegradation of Secondary Organic Aerosols by Long-Term Exposure to Solar Actinic Radiation. *ACS Earth Space Chem.* **2020**, *4*, 1078–1089.
- (29) Fleming, L. T.; Lin, P.; Roberts, J. M.; Selimovic, V.; Yokelson, R.; Laskin, J.; Laskin, A.; Nizkorodov, S. A. Molecular Composition and Photochemical Lifetimes of Brown Carbon Chromophores in Biomass Burning Organic Aerosol. *Atmos. Chem. Phys.* **2020**, 20, 1105–1129.
- (30) Forrister, H.; Liu, J.; Scheuer, E.; Dibb, J.; Ziemba, L.; Thornhill, K. L.; Anderson, B.; Diskin, G.; Perring, A. E.; Schwarz, J. P.; Campuzano-Jost, P.; Day, D. A.; Palm, B. B.; Jimenez, J. L.; Nenes, A.; Weber, R. J. Evolution of Brown Carbon in Wildfire Plumes. *Geophys. Res. Lett.* **2015**, *42*, 4623–4630.
- (31) Saleh, R.; Robinson, E. S.; Tkacik, D. S.; Ahern, A. T.; Liu, S.; Aiken, A. C.; Sullivan, R. C.; Presto, A. A.; Dubey, M. K.; Yokelson, R. J.; Donahue, N. M.; Robinson, A. L. Brownness of Organics in Aerosols from Biomass Burning Linked to Their Black Carbon Content. *Nat. Geosci.* 2014, 7, 647–650.
- (32) Lack, D. A.; Bahreini, R.; Langridge, J. M.; Gilman, J. B.; Middlebrook, A. M. Brown Carbon Absorption Linked to Organic Mass Tracers in Biomass Burning Particles. *Atmos. Chem. Phys.* **2013**, 13, 2415–2422.
- (33) Robinson, M. A.; Decker, Z. C. J.; Barsanti, K. C.; Coggon, M. M.; Flocke, F. M.; Franchin, A.; Fredrickson, C. D.; Gilman, J. B.; Gkatzelis, G. I.; Holmes, C. D.; Lamplugh, A.; Lavi, A.; Middlebrook, A. M.; Montzka, D. M.; Palm, B. B.; Peischl, J.; Pierce, B.; Schwantes, R. H.; Sekimoto, K.; Selimovic, V.; Tyndall, G. S.; Thornton, J. A.; Van Rooy, P.; Warneke, C.; Weinheimer, A. J.; Brown, S. S. Variability and Time of Day Dependence of Ozone Photochemistry in Western Wildfire Plumes. *Environ. Sci. Technol.* **2021**, *55*, 10280–10290.
- (34) Decker, Z. C. J.; Robinson, M. A.; Barsanti, K. C.; Bourgeois, I.; Coggon, M. M.; DiGangi, J. P.; Diskin, G. S.; Flocke, F. M.; Franchin, A.; Fredrickson, C. D.; Gkatzelis, G. I.; Hall, S. R.; Halliday, H.; Holmes, C. D.; Huey, L. G.; Lee, Y. R.; Lindaas, J.; Middlebrook, A. M.; Montzka, D. D.; Moore, R.; Neuman, J. A.; Nowak, J. B.; Palm, B. B.; Peischl, J.; Piel, F.; Rickly, P. S.; Rollins, A. W.; Ryerson, T. B.; Schwantes, R. H.; Sekimoto, K.; Thornhill, L.; Thornton, J. A.; Tyndall, G. S.; Ullmann, K.; Van Rooy, P.; Veres, P. R.; Warneke, C.; Washenfelder, R. A.; Weinheimer, A. J.; Wiggins, E.; Winstead, E.; Wisthaler, A.; Womack, C.; Brown, S. S. Nighttime and Daytime Dark Oxidation Chemistry in Wildfire Plumes: An Observation and Model

- Analysis of FIREX-AQ Aircraft Data. Atmos. Chem. Phys. 2021, 21, 16293-16317.
- (35) Zhang, X.; Ortega, J.; Huang, Y.; Shertz, S.; Tyndall, G. S.; Orlando, J. J. A Steady-State Continuous Flow Chamber for the Study of Daytime and Nighttime Chemistry under Atmospherically Relevant NO Levels. *Atmos. Meas. Tech.* **2018**, *11*, 2537–2551.
- (36) DeCarlo, P. F.; Kimmel, J. R.; Trimborn, A.; Northway, M. J.; Jayne, J. T.; Aiken, A. C.; Gonin, M.; Fuhrer, K.; Horvath, T.; Docherty, K. S.; Worsnop, D. R.; Jimenez, J. L. Field-Deployable, High-Resolution, Time-of-Flight Aerosol Mass Spectrometer. *Anal. Chem.* **2006**, *78*, 8281–8289.
- (37) Ng, N. L.; Herndon, S. C.; Trimborn, A.; Canagaratna, M. R.; Croteau, P. L.; Onasch, T. B.; Sueper, D.; Worsnop, D. R.; Zhang, Q.; Sun, Y. L.; Jayne, J. T. An Aerosol Chemical Speciation Monitor (ACSM) for Routine Monitoring of the Composition and Mass Concentrations of Ambient Aerosol. *Aerosol Sci. Technol.* **2011**, 45, 780–794.
- (38) Nault, B. A.; Campuzano-Jost, P.; Day, D. A.; Schroder, J. C.; Anderson, B.; Beyersdorf, A. J.; Blake, D. R.; Brune, W. H.; Choi, Y.; Corr, C. A.; de Gouw, J. A.; Dibb, J.; DiGangi, J. P.; Diskin, G. S.; Fried, A.; Huey, L. G.; Kim, M. J.; Knote, C. J.; Lamb, K. D.; Lee, T.; Park, T.; Pusede, S. E.; Scheuer, E.; Thornhill, K. L.; Woo, J.-H.; Jimenez, J. L. Secondary Organic Aerosol Production from Local Emissions Dominates the Organic Aerosol Budget over Seoul, South Korea, during KORUS-AQ. Atmos. Chem. Phys. 2018, 18, 17769—17800.
- (39) Guo, H.; Campuzano-Jost, P.; Nault, B. A.; Day, D. A.; Schroder, J. C.; Kim, D.; Dibb, J. E.; Dollner, M.; Weinzierl, B.; Jimenez, J. L. The Importance of Size Ranges in Aerosol Instrument Intercomparisons: A Case Study for the Atmospheric Tomography Mission. *Atmos. Meas. Tech.* **2021**, *14*, 3631–3655.
- (40) Brown, S. S.; An, H.; Lee, M.; Park, J.-H.; Lee, S.-D.; Fibiger, D. L.; McDuffie, E. E.; Dubé, W. P.; Wagner, N. L.; Min, K.-E. Cavity Enhanced Spectroscopy for Measurement of Nitrogen Oxides in the Anthropocene: Results from the Seoul Tower during MAPS 2015. *Faraday Discuss.* **2017**, 200, 529–557.
- (41) Foster, K.; Pokhrel, R.; Burkhart, M.; Murphy, S. A Novel Approach to Calibrating a Photoacoustic Absorption Spectrometer Using Polydisperse Absorbing Aerosol. *Atmos. Meas. Tech.* **2019**, *12*, 3351–3363.
- (42) Zeng, L.; Sullivan, A. P.; Washenfelder, R. A.; Dibb, J.; Scheuer, E.; Campos, T. L.; Katich, J. M.; Levin, E.; Robinson, M. A.; Weber, R. J. Assessment of Online Water-Soluble Brown Carbon Measuring Systems for Aircraft Sampling. *Atmos. Meas. Tech.* **2021**, *14*, 6357–6378
- (43) Lee, B. H.; Lopez-Hilfiker, F. D.; Mohr, C.; Kurtén, T.; Worsnop, D. R.; Thornton, J. A. An Iodide-Adduct High-Resolution Time-of-Flight Chemical-Ionization Mass Spectrometer: Application to Atmospheric Inorganic and Organic Compounds. *Environ. Sci. Technol.* **2014**, *48*, 6309–6317.
- (44) Lopez-Hilfiker, F. D.; Mohr, C.; Ehn, M.; Rubach, F.; Kleist, E.; Wildt, J.; Mentel, ThF.; Lutz, A.; Hallquist, M.; Worsnop, D.; Thornton, J. A. A Novel Method for Online Analysis of Gas and Particle Composition: Description and Evaluation of a Filter Inlet for Gases and AEROsols (FIGAERO). *Atmos. Meas. Tech.* **2014**, *7*, 983–1001.
- (45) Palm, B. B.; Liu, X.; Jimenez, J. L.; Thornton, J. A. Performance of a New Coaxial Ion–Molecule Reaction Region for Low-Pressure Chemical Ionization Mass Spectrometry with Reduced Instrument Wall Interactions. *Atmos. Meas. Tech.* **2019**, *12*, 5829–5844.
- (46) Cox, R. A.; Derwent, R. G. The Ultra-Violet Absorption Spectrum of Gaseous Nitrous Acid. *J. Photochem.* **1976**, *6*, 23–34.
- (47) Zein, A. E.; Coeur, C.; Obeid, E.; Lauraguais, A.; Fagniez, T. Reaction Kinetics of Catechol (1,2-Benzenediol) and Guaiacol (2-Methoxyphenol) with Ozone. *J. Phys. Chem. A* **2015**, *119*, 6759–6765.
- (48) Schobesberger, S.; D'Ambro, E. L.; Lopez-Hilfiker, F. D.; Mohr, C.; Thornton, J. A. A Model Framework to Retrieve Thermodynamic and Kinetic Properties of Organic Aerosol from Composition-

- Resolved Thermal Desorption Measurements. *Atmos. Chem. Phys.* **2018**, *18*, 14757–14785.
- (49) Hallquist, M.; Wenger, J. C.; Baltensperger, U.; Rudich, Y.; Simpson, D.; Claeys, M.; Dommen, J.; Donahue, N. M.; George, C.; Goldstein, A. H.; Hamilton, J. F.; Herrmann, H.; Hoffmann, T.; Iinuma, Y.; Jang, M.; Jenkin, M. E.; Jimenez, J. L.; Kiendler-Scharr, A.; Maenhaut, W.; McFiggans, G.; Mentel, ThF.; Monod, A.; Prévôt, A. S. H.; Seinfeld, J. H.; Surratt, J. D.; Szmigielski, R.; Wildt, J. The Formation, Properties and Impact of Secondary Organic Aerosol: Current and Emerging Issues. *Atmos. Chem. Phys.* **2009**, *9*, 5155–5236.
- (50) Pankow, J. F. An Absorption Model of the Gas/Aerosol Partitioning Involved in the Formation of Secondary Organic Aerosol. *Atmos. Environ.* **1994**, 28, 189–193.
- (51) Donahue, N. M.; Robinson, A. L.; Stanier, C. O.; Pandis, S. N. Coupled Partitioning, Dilution, and Chemical Aging of Semivolatile Organics. *Environ. Sci. Technol.* **2006**, *40*, 2635–2643.
- (\$2) Odum, J. R.; Hoffman, T.; Bowman, F.; Collins, D.; Flagan, R. C.; Seinfeld, J. H. Gas/Particle Partitioning and Secondary Organic Aerosol Yields. *Environ. Sci. Technol.* **1996**, *30*, 2580–2585.
- (53) Lopez-Hilfiker, F. D.; Mohr, C.; Ehn, M.; Rubach, F.; Kleist, E.; Wildt, J.; Mentel, ThF.; Carrasquillo, A. J.; Daumit, K. E.; Hunter, J. F.; Kroll, J. H.; Worsnop, D. R.; Thornton, J. A. Phase Partitioning and Volatility of Secondary Organic Aerosol Components Formed from  $\alpha$ -Pinene Ozonolysis and OH Oxidation: The Importance of Accretion Products and Other Low Volatility Compounds. *Atmos. Chem. Phys.* **2015**, *15*, 7765–7776.
- (54) Lopez-Hilfiker, F. D.; Mohr, C.; D'Ambro, E. L.; Lutz, A.; Riedel, T. P.; Gaston, C. J.; Iyer, S.; Zhang, Z.; Gold, A.; Surratt, J. D.; Lee, B. H.; Kurten, T.; Hu, W. W.; Jimenez, J.; Hallquist, M.; Thornton, J. A. Molecular Composition and Volatility of Organic Aerosol in the Southeastern U.S.: Implications for IEPOX Derived SOA. *Environ. Sci. Technol.* **2016**, *50*, 2200–2209.
- (55) Stark, H.; Yatavelli, R. L. N.; Thompson, S. L.; Kang, H.; Krechmer, J. E.; Kimmel, J. R.; Palm, B. B.; Hu, W.; Hayes, P. L.; Day, D. A.; Campuzano-Jost, P.; Canagaratna, M. R.; Jayne, J. T.; Worsnop, D. R.; Jimenez, J. L. Impact of Thermal Decomposition on Thermal Desorption Instruments: Advantage of Thermogram Analysis for Quantifying Volatility Distributions of Organic Species. *Environ. Sci. Technol.* 2017, 51, 8491–8500.
- (56) Compernolle, S.; Ceulemans, K.; Müller, J.-F. EVAPORA-TION: A New Vapour Pressure Estimation Methodfor Organic Molecules Including Non-Additivity and Intramolecular Interactions. *Atmos. Chem. Phys.* **2011**, *11*, 9431–9450.
- (57) Myrdal, P. B.; Yalkowsky, S. H. Estimating Pure Component Vapor Pressures of Complex Organic Molecules. *Ind. Eng. Chem. Res.* **1997**, *36*, 2494–2499.
- (58) Nannoolal, Y.; Rarey, J.; Ramjugernath, D. Estimation of Pure Component Properties. Fluid Phase Equilib. 2008, 269, 117–133.
- (59) Pankow, J. F.; Asher, W. E. SIMPOL.1: A Simple Group Contribution Method for Predicting Vapor Pressures and Enthalpies of Vaporization of Multifunctional Organic Compounds. *Atmos. Chem. Phys.* **2008**, *8*, 2773–2796.
- (60) Nannoolal, Y.; Rarey, J.; Ramjugernath, D.; Cordes, W. Estimation of Pure Component Properties. *Fluid Phase Equilib.* **2004**, 226, 45–63.
- (61) Joback, K. G.; Reid, R. C. ESTIMATION OF PURE-COMPONENT PROPERTIES FROM GROUP-CONTRIBUTIONS. Chem. Eng. Commun. 1987, 57, 233–243.
- (62) Stein, S. E.; Brown, R. L. Estimation of Normal Boiling Points from Group Contributions. *J. Chem. Inf. Comput. Sci.* **1994**, 34, 581–587
- (63) O'Meara, S.; Booth, A. M.; Barley, M. H.; Topping, D.; McFiggans, G. An Assessment of Vapour Pressure Estimation Methods. *Phys. Chem. Chem. Phys.* **2014**, *16*, 19453–19469.
- (64) Garofalo, L. A.; He, Y.; Jathar, S. H.; Pierce, J. R.; Fredrickson, C. D.; Palm, B. B.; Thornton, J. A.; Mahrt, F.; Crescenzo, G. V.; Bertram, A. K.; Draper, D. C.; Fry, J. L.; Orlando, J.; Zhang, X.; Farmer, D. K. Heterogeneous Nucleation Drives Particle Size

- Segregation in Sequential Ozone and Nitrate Radical Oxidation of Catechol. *Environ. Sci. Technol.* **2021**, *55*, 15637–15645.
- (65) Song, C.; Zaveri, R. A.; Shilling, J. E.; Alexander, M. L.; Newburn, M. Effect of Hydrophilic Organic Seed Aerosols on Secondary Organic Aerosol Formation from Ozonolysis of  $\alpha$ -Pinene. *Environ. Sci. Technol.* **2011**, 45, 7323–7329.
- (66) Lindaas, J.; Pollack, I. B.; Garofalo, L. A.; Pothier, M. A.; Farmer, D. K.; Kreidenweis, S. M.; Campos, T. L.; Flocke, F.; Weinheimer, A. J.; Montzka, D. D.; Tyndall, G. S.; Palm, B. B.; Peng, Q.; Thornton, J. A.; Permar, W.; Wielgasz, C.; Hu, L.; Ottmar, R. D.; Restaino, J. C.; Hudak, A. T.; Ku, I.; Zhou, Y.; Sive, B. C.; Sullivan, A.; Collett, J. L.; Fischer, E. V. Emissions of Reactive Nitrogen From Western U.S. Wildfires During Summer 2018. *J. Geophys. Res.* 2021, 126, No. e2020JD032657.
- (67) Bidleman, T. F. Atmospheric Processes. Environ. Sci. Technol. 1988, 22, 361–367.
- (68) Booth, A. M.; Bannan, T.; McGillen, M. R.; Barley, M. H.; Topping, D. O.; McFiggans, G.; Percival, C. J. The Role of Ortho, Meta, Para Isomerism in Measured Solid State and Derived Sub-Cooled Liquid Vapour Pressures of Substituted Benzoic Acids. RSC Adv. 2012, 2, 4430.
- (69) Chuang, W. K.; Donahue, N. M. A Two-Dimensional Volatility Basis Set Part 3: Prognostic Modeling and NOx Dependence. *Atmos. Chem. Phys.* **2016**, *16*, 123–134.
- (70) Zhao, R.; Lee, A. K. Y.; Huang, L.; Li, X.; Yang, F.; Abbatt, J. P. D. Photochemical Processing of Aqueous Atmospheric Brown Carbon. *Atmos. Chem. Phys.* **2015**, *15*, 6087–6100.
- (71) Cornard, J.-P.; Rasmiwetti; Merlin, J.-C. Molecular Structure and Spectroscopic Properties of 4-Nitrocatechol at Different PH: UV-Visible, Raman, DFT and TD-DFT Calculations. *Chem. Phys.* **2005**, 309, 239–249.
- (72) Hems, R. F.; Abbatt, J. P. D. Aqueous Phase Photo-Oxidation of Brown Carbon Nitrophenols: Reaction Kinetics, Mechanism, and Evolution of Light Absorption. ACS Earth Space Chem. **2018**, 2, 225–234
- (73) D'Ambro, E. L.; Møller, K. H.; Lopez-Hilfiker, F. D.; Schobesberger, S.; Liu, J.; Shilling, J. E.; Lee, B. H.; Kjaergaard, H. G.; Thornton, J. A. Isomerization of Second-Generation Isoprene Peroxy Radicals: Epoxide Formation and Implications for Secondary Organic Aerosol Yields. *Environ. Sci. Technol.* **2017**, *51*, 4978–4987.
- (74) Pye, H. O. T.; Zuend, A.; Fry, J. L.; Isaacman-VanWertz, G.; Capps, S. L.; Appel, K. W.; Foroutan, H.; Xu, L.; Ng, N. L.; Goldstein, A. H. Coupling of Organic and Inorganic Aerosol Systems and the Effect on Gas-Particle Partitioning in the Southeastern US. *Atmos. Chem. Phys.* **2018**, *18*, 357–370.
- (75) Gatzsche, K.; Iinuma, Y.; Tilgner, A.; Mutzel, A.; Berndt, T.; Wolke, R. Kinetic Modeling Studies of SOA Formation from Alpha-Pinene Ozonolysis. *Atmos. Chem. Phys.* **2017**, *17*, 13187–13211.
- (76) Chen, Q.; Liu, Y.; Donahue, N. M.; Shilling, J. E.; Martin, S. T. Particle-Phase Chemistry of Secondary Organic Material: Modeled Compared to Measured O:C and H:C Elemental Ratios Provide Constraints. *Environ. Sci. Technol.* **2011**, *45*, 4763–4770.
- (77) Ruggeri, G.; Bernhard, F. A.; Henderson, B. H.; Takahama, S. Model—Measurement Comparison of Functional Group Abundance in Alpha-Pinene and 1,3,5-Trimethylbenzene Secondary Organic Aerosol Formation. *Atmos. Chem. Phys.* **2016**, *16*, 8729—8747.
- (78) McDonald, B. C.; de Gouw, J. A.; Gilman, J. B.; Jathar, S. H.; Akherati, A.; Cappa, C. D.; Jimenez, J. L.; Lee-Taylor, J.; Hayes, P. L.; McKeen, S. A.; Cui, Y. Y.; Kim, S.-W.; Gentner, D. R.; Isaacman-VanWertz, G.; Goldstein, A. H.; Harley, R. A.; Frost, G. J.; Roberts, J. M.; Ryerson, T. B.; Trainer, M. Volatile Chemical Products Emerging as Largest Petrochemical Source of Urban Organic Emissions. *Science* 2018, 359, 760–764.